Effects of noise on the dc and far-infrared Josephson effect in small-area superconducting tunnel junctions

W. C. Danchi,* J. Bindslev Hansen,† M. Octavio,‡ F. Habbal,§ and M. Tinkham
Physics Department and Division of Applied Sciences, Harvard University, Cambridge, Massachusetts 02138
(Received 13 April 1984)

We report investigations of the effect of noise on the Josephson effect in small-area tunnel junctions, both at dc and when the junction is irradiated by 604-GHz laser radiation. The junctions were made of Sn-SnO-Pb layers of $\sim 1\ \mu m^2$ area, fabricated on crystal quartz substrates with integral planar resonant dipole antennas. The observed systematic falloff of the I_cR_n product with increasing resistance can be accounted for by the thermal activation model (transition-state theory) if an effective noise temperature (presumably extrinsic) of 8 ± 1 K is assumed. The noise rounding of the high-voltage steps can be fitted with the analytic results obtained by P. A. Lee [J. Appl. Phys. **42**, 325 (1971)] for an overdamped junction, but using a fictitious elevated noise temperature of $\sim eV/k$ ($\sim$20—30 K for typical steps at ~ 5 mV) to incorporate the nonthermal shot noise as an effective increase in noise temperature. We have also developed a computer simulation which builds in the effects of the nonlinear quasiparticle resistance of the junctions as well as the voltage-dependent shot noise; it can account for the entire I-V curve, including the photon-assisted tunneling steps. Noise currents are found to have much less effect on the finite-voltage Josephson steps than in reducing the I_cR_n product, which explains the anomalously high ratios of step widths to measured I_c that are found experimentally.

I. INTRODUCTION

The possibility of using Josephson junctions as high-frequency detectors has been the subject of interest in recent years.[1] For a practical device, a quantitative knowledge of the effects of various noise sources on junction behavior is required. Most of the experimental work on noise in Josephson junctions has been devoted to understanding thermal noise in low-capacitance metallic-like junctions,[2–4] or $1/f$ noise[5,6] and zero-point fluctuations[7] in shunted tunnel junctions. Classic measurements of the effect of noise in unshunted tunnel junctions have been performed by Fulton and Dunkleberger[8] on large-area junctions, and more recently by Voss and Webb[9] and by Jackel *et al.*[10] on smaller-area junctions.

In order for a tunnel junction to be useable in detector applications at very high frequencies, e.g., in the far-infrared (FIR) region of the spectrum, it must have low capacitance and high normal-state resistance for efficient coupling to the incident radiation field. High junction capacitance has limited the use of Josephson junctions for submillimeter wave-detector applications, but recent improvements in fabrication techniques have made it possible to fabricate small-area tunnel junctions with high resistance, reasonably low capacitance, and good FIR response.[11,12]

In this paper we present a detailed analysis of the effects of noise, both thermal Johnson noise and shot noise, on the current-voltage (I-V) characteristics of small-area superconducting tunnel junctions which we have shown in previous work to have good Josephson response at 604 GHz (496 μm). In Sec. II we begin with a brief review of the experimental techniques used to fabricate the junctions and to couple them to the FIR radiation from a homemade FIR laser. Next, in Sec. III we describe briefly the observed response of the junctions both without and with irradiation from the FIR laser source.

Following this, in Sec. IV we present the results of two analytic approximations and of computer simulations of the effects of noise on the I-V characteristics. First, we derive an approximate formula which provides a simple explicit dependence of the measured noise-reduced critical current on the effective noise temperature and the bias-current sweep rate. Second, we present results using the Lee approximation to characterize the noise rounding of the (nonhysteretic) high-voltage ac Josephson steps, using an elevated noise temperature (typically 20—30 K), attributed to shot noise at finite voltage.

We then present the results of a computer simulation based on a modified RSJ (resistively shunted junction) model, which includes the effect of the voltage-dependent (shot) noise as well as the nonlinear quasiparticle resistance of the junctions and the associated photon-assisted tunneling structure. This approach allows us to calculate the entire I-V curve, including the effect of noise in reducing I_c and in rounding the ac Josephson effect steps. The computer simulations are compared with the results obtained on the basis of the analytic approximations and with the experimental data. We end the paper with a brief summary and discussion of this work.

II. EXPERIMENTAL TECHNIQUES

Two sets of small-area Sn-SnO-Pb superconducting tunnel junctions were fabricated during the course of this work. The first set was fabricated using the original overlap junction technique of Dolan[13] and Dunkleberger.[14] These junctions had relatively low resistance ($R_n \sim 1.5$ —12.5 Ω) and large area [(1.5—7.0)$\times 10^{-8}$ cm^2], and were used primarily to characterize the dc electrical properties

of the junctions, i.e., the temperature dependence of the superconducting energy gap of Sn, $\Delta_{Sn}(T)$, and the temperature dependence of the critical current $I_c(T)$. The junctions of the second set were measured in the far-infrared and were fabricated by the resist-aligned technique of Howard *et al.*,[15] except for one that was fabricated by the edge-aligned technique.[15] Resistances of these junctions ranged from ~ 16 to 1600 Ω, and areas varied from 0.4×10^{-8} cm^2 to 2.4×10^{-8} cm^2.

In order to perform the sequence of metal-film depositions and glow-discharge oxidation which are used in the three junction fabrication techniques, we first prepared bridges of photoresist suspended above the surface of the single-crystal quartz substrates. The evaporation and oxidation sequence for the overlap junction begins with the deposition of the base-electrode material (Sn) at an angle to the substrate normal ($+55°$), is followed by a glow-discharge oxidation of the base electrode, and ends with the evaporation of the counter electrode (Pb) at an angle of $-50°$. For this evaporation sequence, the substrates were placed on a rotable sample holder which was cooled to liquid-nitrogen temperature in a cyropumped evaporator at a base pressure of 2×10^{-7} Torr. The Sn base electrode was oxidized by a dc glow discharge in 99.9999%-pure oxygen at a pressure of 30 mTorr for 30–60 sec with 12 mA of current at 1.1 kV.

In the resist-aligned sequence, the area of the junction is reduced from that of the overlap junction by the deposition of an insulating layer of Ge after the base-electrode deposition at an angle ($\sim +42°$, for example) which is slightly less than the angle of the base-electrode deposition. The final variant of the overlap technique, the edge-aligned technique, begins with the evaporation of Sn at normal incidence. The Ge layer is evaporated at an angle such that it breaks over the Sn edge; the junction is glow-discharge oxidized as before, and the Pb counter electrode is evaporated at a shallow angle to insure it touches the Sn-SnO surface.

Far-infrared radiation does not couple significantly to small-area tunnel junctions alone. A suitable scheme to couple the FIR radiation from a FIR laser source to the junction was found, and is described in the following paragraphs. In short, radiation from a FIR laser source was focused by an $f/4$ TPX lens and an electroformed copper cone to a small-area tunnel junction at the center of a dipole antenna on the backside of the sample substrate. Figure 1 illustrates the complete coupling arrangement, seen in cross section, as viewed in the transverse-optical access Dewar. We now give a more detailed description.

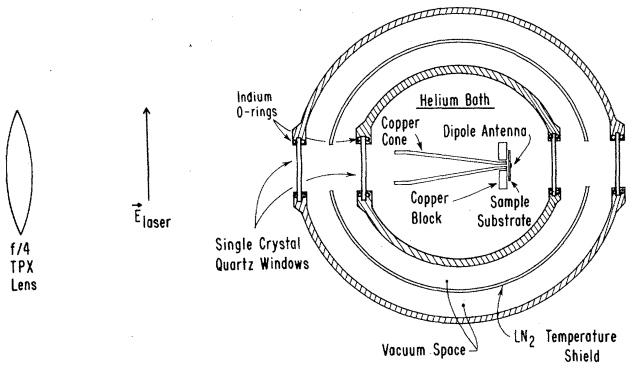

FIG. 1. Detail of transverse-optical access Dewar. FIR laser radiation is focused by the TPX lens onto the cone, through the backside of the substrate, onto the junction-antenna structure.

The antenna was fabricated following the design rules developed by Mizuno *et al.*[16] Z-cut crystal quartz substrates, of thickness $t=2.54\times10^{-2}$ cm, were used. Such quartz has a refractive index $n=2.3$ in the 100 μm to 1.2 mm wavelength region of interest to this experiment. Accordingly, it is useful to define an effective thickness, $t_{\text{eff}}=nt/\lambda$, where λ is the free-space wavelength. For the 496-μm methyl fluoride (CH_3F) laser line, $t_{\text{eff}}=1.2$ for our substrates, decreasing to $t_{\text{eff}}=0.498$ for the 1.22-mm isotopic methyl fluoride ($^{13}CH_3F$) laser line. To take account of n and these t_{eff} values, the antenna length was shortened to 77% of its free-space resonant length (0.48λ) to 0.37λ, or $l_{\text{res}}=183$ μm for the 496-μm line and $l_{\text{res}}=451$ μm for the 1.22-mm line.

A conical horn with a short cylindrical waveguide section was used as a feed for the dipole antenna. The design of this horn was based on work of Blaney.[17] The horn had a conical section 35 mm in length, an opening 11.4 mm in diameter, and an opening angle of $\sim 18°$. The waveguide section was 7 mm long and 0.79 mm in diameter. This cone was fabricated by electrodeposition of copper on a polished stainless-steel mandrel, in order to keep the surface roughness to a minimum. The cone has a calculated gain of 29 dB, or a factor of 760, over that of an isotropic radiator.[18] The waveguide section had a cutoff wavelength of 1.35 mm for the TE_{11} mode, the lowest order or dominant mode. Cutoff wavelengths for some higher-order modes are 1.03 mm for the TM_{01} mode, 0.81 mm for the TE_{21} mode, 0.65 mm for the TM_{11} and TE_{01} modes, etc.[19] Therefore, although the waveguide could only operate in the fundamental mode at the 1.22-mm laser line, at shorter wavelengths, such as the strong 496-μm line, unfortunately several modes could be excited at once.

In this work no attempt was made to resonate out the junction reactance by tuning stubs or plungers, as is commonly done at longer wavelengths. However, the coupling arrangement used in this experiment, in which the radiation is focused through to the backside of the substrate, takes advantage of the effect of the dielectric substrate on the antenna pattern. During a run, the cone and sample block could be rotated slightly about the center line of the Dewar to optimize the coupling of the radiation to the junction.

The FIR radiation came from a homemade optically pumped FIR laser.[20] Although the characteristics of this laser have been thoroughly described before, they will be summarized here.

Figure 2 displays the complete FIR laser system. A modified commercial CO_2 laser (Apollo model 550L) provided the pump beam. The pump laser had a 12-mm diam, 1.8-m long cavity, with its active region enclosed by two ZnSe Brewster angle windows. This laser had been

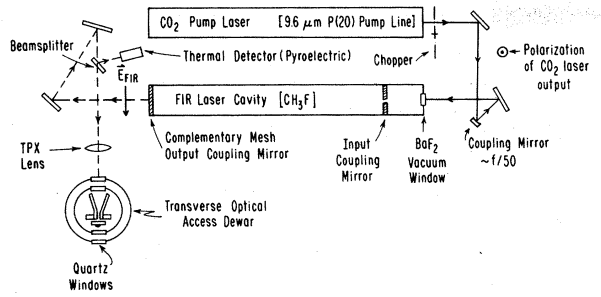

FIG. 2. Optically pumped FIR laser setup.

modified in two ways. First, the cavity was ~20 cm longer than usual for increased output power; second, the output coupling mirror from the end of the laser cavity was removed and was replaced by a second Brewster angle window. A 75 lines/mm grating was used to tune the laser to a single line, and also served as one end mirror. The semitransparent output coupling mirror was mounted on a piezoelectric tranducer (PZT) stack for fine tuning of the operating frequency, and had a 20-m radius of curvature. The laser was mounted on a granite slab and enclosed by a metal cover for stability against frequency drift due to thermally induced cavity-length changes. In the typical operation of the laser, 12–25 W of output power could be achieved over the 9.5-μm band, with a nearly Gaussian output beam.

The FIR cavity consisted of a 38-mm-diam, 3-m-long Pyrex pipe with two flat end mirrors. The CO_2-laser beam was focused into the FIR cavity by an $f/50$ coupling mirror through a BaF_2 window, and through a 3-mm-diam hole in the input coupling mirror mounted at the end of the dielectric waveguide. This mirror was mounted on a translation stage between two stainless-steel-bellows vacuum seals. This mirror and also the output coupling mirror were on gimbal mountings for adjustment of the cavity finesse (essentially the cavity quality factor Q). The mirror could be translated to adjust the cavity length to the proper resonant FIR cavity mode. The output coupling mirror consisted of an Al thin-film, capacitive (or complementary) mesh[20,21] on a 2-mm-thick, 1.75-in.-diam, optically polished single-crystal quartz flat.

The FIR radiation is transformed from the EH_{11} cavity mode to the TEM_{00} Gaussian free-space mode upon transmission through the output coupling mirror. The radiation is reflected by two mirrors and then the reflected beam from the single-crystal quartz (flat) beam splitter feeds the pyroelectric detector (Molectron model P4-73). The transmitted beam is focused by an $f/4$ lens of TPX or polyethylene, through room temperature and liquid-helium temperature single-crystal quartz windows onto the electroformed copper feed horn, described above.

The FIR laser performed best when the laser room was warm, ~80 °F, and when the CO_2 laser had been warmed up for 2–3 h before use. The FIR cavity was always operated in a sealed-off mode at the pressure (~100 mTorr) which gave the maximum output power. Under these conditions the FIR output was very stable, having long-term drifts of at most ~10% in 24 min of operation, using only this passive stabilization scheme. Short-term fluctuations were ~2–3 %, measured with a 0.3-sec time constant. Before I-V curves of the irradiated junction were recorded, the FIR laser was adjusted for maximum power and stability. I-V curves could then be measured at different laser powers by inserting Mylar or Plexiglass absorbers at the output of the FIR laser.

The voltage of the junction was measured by a battery-powered Princeton Applied Research model-113 (PAR-113) preamplifier, while the current from a battery-powered current source was measured by monitoring the voltage across a precision resistor (typically 100 Ω) also using a battery-powered PAR-113 preamplifier. All the dc lead wires were brought down into the Dewar through low-pass rf filters (with ~1-kHz cutoff frequency) at the top of the Dewar, and all lead wires were terminated with 500-Ω metal-film resistors in the bath before they were connected to the sample. The lead wires were connected to thin-film sample pads (~1 mm in diameter), using pressed-indium contacts.

III. EXPERIMENTAL RESULTS

A. dc characteristics

The basic junction parameters needed for our subsequent analysis are I_c^0, R_n, and C. The measured I_c, however, is reduced below the intrinsic value I_c^0 by noise-rounding effects. This I_c^0 is expected to scale as R_n^{-1}, so that $I_c^0 R_n$ is independent of R_n, and at low temperatures, is of the order of the energy gap Δ, which can be measured directly from structure on the I-V curves. A number of the measured (or inferred) parameter values for several low-resistance junctions are listed in Table I. The eight samples shown in the table had resistances R_n ranging from 1.5 to 12.5 Ω, areas A from 1.5 to 6.9 $(\mu m)^2$, and critical-current densities J_c from 2×10^3 to 2.6×10^4 A/cm^2. Table I also lists the I_cR_n products at $T=1.4$ K which range from 0.40 to 1.28 mV. The lowest (0.40 mV) was for the highest-resistance sample, while for samples below 4 Ω, the I_cR_n products were high, >1.0 mV, and did not correlate with sample resistance. Finally the table also gives estimates of the junction capacitances C, as well as the Stewart-McCumber parameter, $\beta_c = 2eI_c^0R_n^2C/\hbar$, and the Josephson plasma frequency $\omega_J = (2eI_c^0/\hbar C)^{1/2} = (\beta_c)^{1/2}/R_nC$.

In Table I the capacitance of each junction is estimated from the formula $C=\epsilon_r(\epsilon_0 A/t)$, where A is the junction area, t is the oxide thickness, ϵ_r is the dielectric constant, and ϵ_0 is the dielectric permittivity of vacuum. The area A is the geometrical area of the junction, estimated from scanning electron microscope (SEM) micrographs, and does not include estimates of parasitic capacitances such as the extra overlap of the Pb layer on the Ge insulating layer visible in SEM micrographs. The relative dielectric constant, $\epsilon_r=6$ for SnO, is estimated from the ratio of the wave velocity in the oxide to that in free space, $\bar{c}/c$, for Sn-SnO-Sn junctions, as measured by other workers.[8,22] For the oxide thickness t we use $t=20$ Å as a nominal value.[23]

The most poorly known junction parameter in Table I

TABLE I. Parameters of low-resistance junctions.

Sample	R_n (Ω)	I_c (μA) ($T=1.4$ K)	A (μm^2)	I_cR_n (mV) ($T=1.4$ K)	C (pF)	β_c (est.)[a]	ω_J (10^{12} sec^{-1}) (est.)[a]	J_c(A/cm^2) (est.)[a]	J_c(A/cm^2) (meas.)[b]
P19	4.0	230	2.0	0.92	0.053	0.77	4.1	1.5×10^4	1.2×10^4
P27	12.5	32	4.6	0.40	0.12	5.5	1.6	2.1×10^3	7.0×10^2
P31	5.0	192	7.0	0.96	0.19	3.5	2.0	3.4×10^3	2.7×10^3
P37	2.4	450	4.5	1.08	0.12	1.1	3.6	1.1×10^4	1.0×10^4
P47A	3.3	380	1.5	1.25	0.040	0.48	5.3	2.4×10^4	2.5×10^4
P47A	2.4	527	1.9	1.26	0.050	0.44	5.5	2.6×10^4	2.8×10^4
P57B	3.6	356	1.6	1.28	0.042	0.55	4.9	2.1×10^4	2.2×10^4
P59	1.5	725	6.9	1.09	0.18	0.98	3.7	1.2×10^4	1.1×10^4

[a]Parameters denoted (est.) are computed using a critical current, $(I_c)_{\text{est.}}$, calculated from the nominal I_cR_n product of 1.2 mV, and the sample resistance, R_n. (See text.)
[b]J_c(meas.) is computed from the measured critical currrent, I_c, in column 3 of this table. (See text.)

is the junction capacitance, and it is difficult to put accurate bounds on its value. The area is known to ~20%, limited by the accuracy of the calibration of the length scale on the SEM, and the accuracy of measuring the area from the SEM micrographs. The relative dielectric constant ϵ_r and the dielectric oxide thickness t are also difficult parameters to quantify. We estimate that the ratio of ϵ_r/t is known only to ~20%, giving a total potential error of ~40% on the values of the capacitances.

The Stewart-McCumber parameter β_c and the plasma frequency ω_J are quantities derived from the critical current, capacitance, and normal-state resistance. Of these parameters, the normal resistance R_n is known to a few percent. The 40% uncertainty in C estimated above translates into a 40% uncertainty in β_c and a 20% uncertainty in ω_J, which scales as $C^{-1/2}$. The measured critical current I_c is known to a few percent, but in the weakly coupled junctions, this value is substantially lower than the intrinsic I_c^0 because of premature noise-induced switching out of the zero-voltage state. Moreover, it is I_c^0 which enters the definitions of β_c and ω_J. Thus we have computed the listed values of these parameters using *estimated* values of I_c^0, based on a nominal $I_c^0R_n$ product at 1.4 K to 1.2±0.1 mV, taken from the mean of the I_cR_n products of the five low-resistance samples P37-P59. This value of the I_cR_n product is close to the theoretical value, 1.30 mV, computed from the relation

$$I_cR_n=\frac{1}{e}\frac{\Delta_1\Delta_2}{\Delta_1+\Delta_2}K\left[\left|\frac{\Delta_1-\Delta_2}{\Delta_1+\Delta_2}\right|\right],$$

assuming $\Delta_{\text{Pb}}(0)=1.31$ meV and $\Delta_{\text{Sn}}(0)=0.57$ meV; here K is the complete elliptic integral of the first kind.

Near T_c, the square of the Sn gap, $(2\Delta_{\text{Sn}})^2$, should be proportional to T_c-T, as can be seen from the BCS expression[24] for the superconducting energy gap,

$$\Delta(T)=1.74\Delta(0)(1-t)^{1/2} \text{ for } T\approx T_c\ , \quad (1)$$

where $t=T/T_c$. Therefore, $\Delta_{\text{Sn}}(0)$ can be inferred from the slope of $\Delta^2(T)$ at T_c, defined as the temperature at which $[2\Delta_{\text{Sn}}(T)]^2$ extrapolates to zero. The data from three of the four samples that were checked give $T_c(\text{Sn})=3.79\pm0.01$ K and $\Delta_{\text{Sn}}(0)=0.56\pm0.03$ meV, while the fourth had $T_c=3.81\pm0.01$ K and $\Delta_{\text{Sn}}(0)=0.47\pm0.03$ meV. The values are close to (and consistent with) nominal values used by other workers,[8,25]

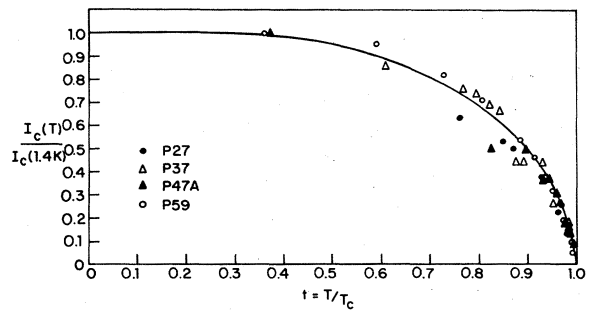

FIG. 3. Critical current at temperature T, normalized to the critical current at 1.4 K, versus the reduced temperature, $t=T/T_c$, for some of the low-resistance junctions.

TABLE II. Parameters of high-resistance junctions measured in the far infrared.

Sample	Laser line (μm)	R_n (Ω)	I_c (μA) ($T=1.4$ K)	A (μm^2)	I_cR_n (mV) ($T=1.4$ K)	C (pF)	β_c (est.)[a]	ω_J (10^{12} sec^{-1}) (est.)[a]	J_c (A/cm^2) (est.)[a]	J_c (A/cm^2) (meas.)[b]
P73	496	16.4	55	2.2	0.90	0.058	3.5	2.0	3.3×10^3	2500
P81	496	24	27	2.4	0.62	0.064	5.6	1.5	2.1×10^3	1100
P89	496	176	1.5	0.40	0.26	0.011	7.0	1.4	1.7×10^3	380
P91a	496	381	0.27	1.7	0.10	0.045	63	0.46	1.9×10^2	16
P91b	1222	330	0.50	2.4	0.17	0.064	77	0.42	1.5×10^2	21
P97	1222	156	1.5	1.9	0.23	0.05	28	0.68	4.0×10^2	79
B11	496	1600	0.08	0.93	0.13	0.025	146	0.30	8.1×10^1	8.6

[a]Parameters denoted (est.) are computed using a critical current, $(I_c)_{\text{est.}}$, calculated from the nominal I_cR_n product of 1.2 mV, and the sample resistance, R_n. (See text.)
[b]J_c(meas.) is computed from the measured critical current, I_c, in column 4 of this table. (See text.)

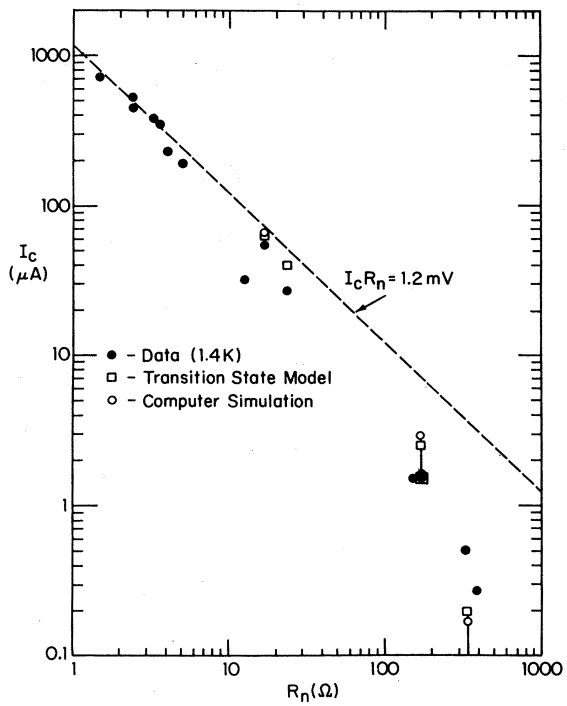

FIG. 4. Critical current I_c at 1.4 K vs normal resistance R_n for junctions studied in this work. For $R_n > 10\ \Omega$, the data (solid circles) fall increasingly below the dashed line which depicts a constant I_cR_n product. Results of the transition-state theory and of computer simulations (see text) are shown in open squares and circles, respectively, for $T_N^{\text{eff}}=7$ and 9 K. For $R_n < 30\ \Omega$, the results for the two noise temperatures agree within the size of the symbol. Where two symbols are visible, the upper corresponds to 7 K, the lower to 9 K. The variance in I_c for given T_N^{eff} is much smaller than the difference in the means for 7 and 9 K, and is not shown.

indicating that the junctions are of good quality.

In the absence of fluctuations the temperature dependence of the critical current should have the same functional form for all junctions having electrodes of the same materials. Figure 3 displays $I_c(T)/I_c(1.4\text{ K})$ versus $t=T/T_c$ for the four junctions discussed in the preceding paragraph. It is clear that the data from all the samples lie close to the same dependence, i.e., the solid line in the figure.

Table II displays the dc characteristics of the samples that were used in the FIR measurements, the results of which will be presented in the next section. The estimated critical-current densities for these junctions vary from 80 A/cm^2 for the 1600-Ω sample, to about 3000 A/cm^2 for the 16-Ω sample; areas ranged from about 0.4×10^{-8} cm^2 to 2.4×10^{-8} cm^2. The analysis of the errors of the various measured quantities of Table I applies as well to Table II. The I_cR_n products vary from the highest values of $\sim$0.9 mV for a junction of resistance of $\sim$16 Ω, decreasing to a value of $\sim$0.10 mV for junctions with resistance $>300\ \Omega$. This falloff of the I_cR_n product with increasing junction resistance is shown in Fig. 4, where the solid circles represent the I_c and R_n data of Tables I and II. The dashed line indicates the roughly constant I_cR_n products

(~ 1.2 mV) of the low-resistance samples. The open circles and squares represent the results of the analytic approximation and computer simulations which will be presented in Sec. IV.

B. Far-infrared response

We have studied the far-infrared response of the junctions of Table II and typical I-V curves are shown in Fig. 5. In the low-resistance, large-area junctions ($R \sim 20\ \Omega$, $A \sim 2\times 10^{-8}$ cm^2), we find flat steps, with very little noise rounding, which fit the simple RSJ step shape very well, as illustrated in Fig. 6. Unfortunately, the low impedance of these junctions causes a severe impedance mismatch between junction and antenna, so that only a small fraction of the FIR power is coupled into the junction and only a few steps are observed. In the particular junction shown in Fig. 5(a), with our highest achieved normalized ac voltage of $2\alpha = 2eV_L/\hbar\omega_L = 1.6$, we observed four Josephson steps and one photon-assisted tunneling step. (Here $\omega_L/2\pi$ is the FIR laser frequency and V_L is the FIR voltage across the junction.)

The behavior of a high-resistance, small-area junction ($R = 176\ \Omega$, $A \sim 0.5\times 10^{-8}$ cm^2) shown in Fig. 5(b), is quite different. Here 2α as high as 8.4 was obtained from the same laser power, and seven Josephson steps and six photon-assisted steps were observed. Notice that in this case, the steps are strongly affected by noise, which causes marked rounding and also a slight tilt (i.e., observable differential resistance) of the steps. The coupling of the radiation to the high-resistance junction is relatively good; it produces steps at voltages as high as 8.75 mV, comparable to the performance (12.5 mV) obtained by Weitz *et al.*,[26,27] using point contacts with long-wire antenna structures and the same laser source. As a consequence of the excellent tunneling characteristics of these junctions, it is possible to identify features, such as the photon-assisted tunneling steps, not observed in point-contact measurements. The variation of the Josephson step widths with laser power has been analyzed in detail,[11] as well as the power dependence of the photon-assisted tunneling steps.[12] In both respects, we found excellent agreement between our data and the theory of the Josephson effect and the Tien-Gordon[28] theory of the photon-assisted tunneling effect, respectively. Detailed analyses of these effects have been presented in our earlier publications.[11,12]

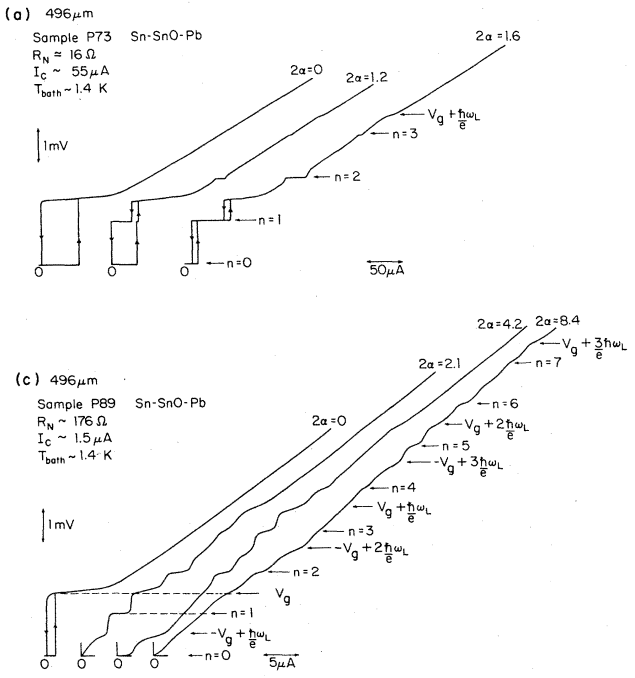

FIG. 5. (a) Typical I-V curves of a low-resistance sample for several laser powers. Here, $V_g = (\Delta_{Pb} + \Delta_{Sn})/e$. (b) Typical I-V curves of a high-resistance junction for several laser powers. The voltage of the first Josephson step is indicated by a dashed line; the I-V curves were taken at power levels given by the maximum of this step width and at subsequent zeros. The current step at the gap is also identified by a dashed line.

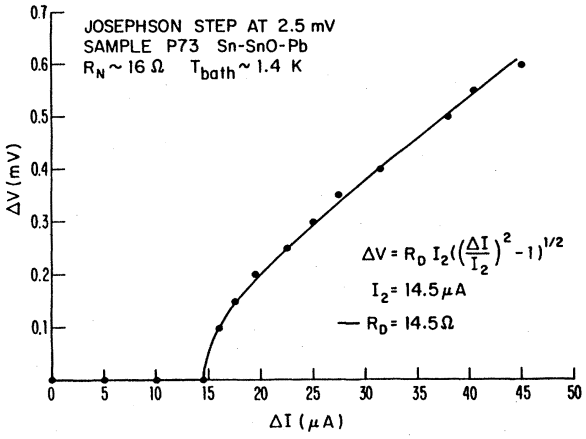

FIG. 6. RSJ-model fit to the shape of the second Josephson step for a 16-Ω junction illuminated with 604-GHz laser radiation.

In these higher-resistance junctions, which give the best coupling to the radiation, the measured I_cR_n product falls increasingly below the theoretical value as R_n increases, the discrepancy reaching a factor of ~ 0.08 in a 381-Ω junction, as shown previously in Fig. 4. The systematic nature of the deviation indicates a fundamental origin. As we shall show in some detail, this reduction of I_c can be naturally explained by noise effects.

Given the large depression of the dc critical current by noise currents, it is clear that they might be expected to affect the higher Josephson steps as well. However, if the effect of the noise in narrowing the finite-voltage steps were significantly less than its effect on the zero-voltage step, that would account for the need to scale up all the theoretical ratios of I_n/I_c by a constant factor (~ 2 for a representative junction) in order to fit to the experimental data.[11] Model calculations reported below support this hypothesis.

IV. COMPARISONS WITH THEORETICAL MODELS

A. Microscopic theory and the RSJ model

According to the microscopic theory of a superconducting tunnel junction,[29] for a constant dc bias voltage V_0,

the total current through the junction is the sum of a quasiparticle term $I_{qp}(V_0,T)$, a pair current term proportional to the sine of the phase difference across the junction with coefficient $I_{J1}(V_0,T)$, and a pair-quasiparticle interference current term proportional to $\cos\phi$:

$$I(t)=I_{qp}(V_0,T)+I_{J1}(V_0,T)\sin\phi+I_{J2}(V_0,T)\cos\phi\ , \tag{2}$$

where $\phi=\phi(t)$ is the phase difference across the junction, T is the junction temperature, and the time dependence of the phase difference can be related to the voltage across the junction by the Josephson relation $2eV(t)/\hbar=\dot{\phi}\equiv d\phi/dt$.

The RSJ (resistively-shunted junction) model can be derived from the microscopic theory by assuming that $I_{J1}(V_0,T)$ is independent of voltage (frequency), so that it can be replaced by the maximum dc supercurrent at the junction temperature $I_c^0(T)$. The quasiparticle current, $I_{qp}(V_0,T)$, is modeled either by using a voltage-dependent conductance $G(V)$, i.e., $I_{qp}=G(V)V$, or more often simply by using the normal-state conductance $G_n=1/R_n$, i.e., $I_{qp}=G_nV$. The $\cos\phi$ term is usually ignored as having minimal observable effect. The external circuitry which drives the junction is modeled as a dc current source, plus a time-dependent (ac) current source at the laser frequency ω_L if appropriate. The effect of the capacitance of the junction is included by a displacement current term, $C\,dV/dt$. The resulting RSJ-model equation is

$$I_T=G(V)V+I_c^0\sin\phi+C\frac{dV}{dt}\ , \tag{3}$$

where $I_c^0=I_c^0(T)$. The total current I_T through the device is written as

$$I_T=I_{dc}+I_L\sin(\omega_L t)+\hat{I}_N(t)\ , \tag{4}$$

where a noise term $\hat{I}_N$ has been included to model noise from the shunt conductance $G(V)$, or an external noise source. Inserting the equation for the junction voltage $V=(\hbar/2e)(d\phi/dt)$ into Eq. (3), the result is

$$\frac{d^2\phi}{dt^2}+G\left[\frac{d\phi}{dt}\right]\frac{1}{C}\frac{d\phi}{dt}+\frac{2eI_c^0}{\hbar C}\sin\phi=\frac{2eI_T}{\hbar C}\ . \tag{5}$$

Equation (5) can be simplified by rewriting it in terms of normalized units. Frequencies are normalized to ω_J, the Josephson plasma frequency. Currents are normalized to I_c^0, the critical current, and voltages to the $I_c^0R_n$ product. The resulting equation is

$$\frac{d^2\phi}{d\tau^2}+g\frac{d\phi}{d\tau}+\sin\phi=\rho_{dc}+\rho_L\sin(\Omega\tau)+\hat{\rho}_N\ , \tag{6}$$

where $\tau=\omega_J t$ is the normalized time and $(d\phi/d\tau)g=I_{qp}(d\phi/d\tau)/I_c^0$ is a function of the normalized frequency (voltage), $d\phi/d\tau$. The normalized ac current and frequency are $\rho_L=I_L/I_c^0$ and $\Omega=\omega_L/\omega_J$, respectively. The noise term is $\hat{\rho}_N=\hat{I}_N/I_c^0$. If $G(V)=(R_n)^{-1}$, then g becomes $(\beta_c)^{-1/2}$.

As often noted before, Eq. (6) also describes a simple mechanical analogy to the Josephson tunnel junction: a ball with mass C, position ϕ, and velocity $\dot{\phi}$ moving on a washboard with a tilt $\propto I$ and subjected to a velocity-dependent frictional force $g(\dot{\phi})\dot{\phi}$. In this analogy the current noise corresponds to a stochastic shaking motion of the washboard which will cause the ball to escape from the stationary state $\langle\dot{\phi}\rangle=0$ in a well on the washboard for a value of the tilt that is smaller than the critical value without noise, I_c^0.

Our approach to solving the RSJ model with noise is twofold. We shall first, in Sec. IV B, use analytic approximations to the solution of the RSJ model [Eq. (6)] and compare the results to the experimental data both for the noise-induced premature switching out of the zero-voltage state (escape from the well) and for the noise rounding of the high-voltage FIR steps in the I-V curves. Secondly, in Sec. IV C, we shall present full I-V curves (with noise) obtained by solving Eq. (6) numerically on a computer and compare these with the data and with the results of the analytical expressions.

B. Analytic approximations

1. *Noise depression of the critical current*

In the limit of small damping (large β_c), Lee[30] showed that the lifetime $\tau(I)$ of the zero-voltage state may be calculated by using a simple thermal activation model, also called the transition-state model:

$$\frac{1}{\tau(I)}=\frac{\omega_A}{2\pi}\exp(-E/kT)\ , \tag{7}$$

where E is the height of the energy barrier:

$$E=E_J^0[\rho(2\sin^{-1}\rho-\pi)+2\cos(\sin^{-1}\rho)]\ ,$$

$E_J^0=\hbar I_c^0/2e$, $\rho=I/I_c^0$, and ω_A is the cylic "attempt" frequency (the resonance frequency for the ball in the well):

$$\omega_A=\omega_J(1-\rho^2)^{1/4}\ . \tag{8}$$

The transition-state model [Eq. (7)] was used successfully by Fulton and Dunkelburger[8] in their study of the lifetime of the zero-voltage state of highly underdamped Sn and Pb tunnel junctions. They noted that for a given sweep rate $\dot{I}$ and $\tau(I)$, the probability for the junction to switch, $P(I)$, at a given current level obeys the relation

$$P(I)=[\tau(I)\dot{I}]^{-1}\left[1-\int_0^I P(u)du\right]\ . \tag{9}$$

This expression is interpreted in terms of an ensemble of junctions subject to increasing current, I. The second factor on the right represents the fraction of junctions remaining in the zero-voltage state when the current has reached value I. This integral equation for $P(I)$ is easily solved by transforming it to a differential equation. By denoting $\tau(I)\dot{I}$ by $\xi(I)$, Eq. (9) can be written as $d[\xi(I)P(I)]/dI=-P(I)$ which has the solution

$$P(I)=\xi^{-1}(I)\exp\left[-\int_0^I\xi^{-1}(I')dI'\right]\ . \tag{10}$$

From Eq. (10) we can obtain the maximum in the probability distribution, which is where the junction is most likely to switch. We will assume $\dot{I}=$const. Differentiating Eq. (10) and setting the result of zero, we obtain

$$\frac{d\tau}{dI}=-1/\dot{I} \tag{11}$$

as the condition for the maximum of $P(I)$. We will now make use of an approximation for $\tau(I)$. Noting that

$$E/kT\simeq\frac{\gamma\sqrt{8}}{3}(1-\rho)^{3/2},$$

with $\gamma=\hbar I_c^0/ekT$, and taking $\omega_A=\omega_J$, i.e., neglecting the $(1-\rho^2)^{1/4}$ factor which has only a small effect over the important range of I for weakly coupled junctions, we obtain

$$\tau(I)=(2\pi/\omega_J)\exp[\sqrt{8}\gamma(1-\rho)^{3/2}/3]. \tag{12}$$

To solve for $\rho=I/I_c^0$ at the maximum of the switching probability distribution, we neglect a term logarithmic in $(1-\rho)$, which is significant only very close to $\rho=1$, and obtain the following expression for the fluctuation-reduced critical current I_c:

$$I_c=I_c^0\left\{1-\left[\left[\frac{3}{\sqrt{8}\gamma}\right]\ln\left[\frac{\omega_J I_c^0}{\pi\sqrt{8}\gamma\dot{I}}\right]\right]^{2/3}\right\}. \tag{13}$$

We compared this simple expression with the results of calculating $\tau(I)$ and $P(I)$ directly, and found good agreement. For example, consider junction P89 which has $\omega_J=1.4\times10^{12}$ sec^{-1} and $I_c^0=6.8\mu$A. If we take $T=9$ K ($\gamma=36$), anticipating the presence of extrinsic noise, Eq. (13) gives $I_c/I_c^0=0.20$, whereas directly finding the maximum in $P(I)$ by numerical integration of Eq. (9) we find $I_c/I_c^0=0.22$. The current sweep rate, $dI/dt=1$ μA/sec, used here is typical for our experiments. The temperature $T=9$ K chosen here, gives a good fit to the experimentally observed value of I_c: $I_c(1.4\text{ K})=1.5$ μA$=0.22I_c^0$ (1.4 K). We take this temperature to be the effective noise temperature, $T_N^{\rm eff}$, seen by the junction. In Fig. 4 we have plotted the bias current at the maximum of $P(I)$, i.e., the most likely critical current from Eq. (13), for five of our junctions using $T_N^{\rm eff}=8\pm1$ K.

We note from Eq. (13) that the reduction of I_c depends logarithmically on the sweep rate $\dot{I}$ as well as directly on the noise temperature through γ. Even the logarithmic dependence is important when comparing laboratory sweep rates with those in computer simulations, which are typically 10^7 times faster for reasonable amounts of computer time. To illustrate, we note that the noise parameters γ required to give the same reduction in I_c at two different sweep rates are related by

$$\frac{\gamma_2}{\gamma_1}=\frac{\ln(\omega_J I_c^0/\sqrt{8}\pi\gamma_2\dot{I}_2)}{\ln(\omega_J I_c^0/\sqrt{8}\pi\gamma_1\dot{I}_1)}. \tag{14}$$

This can be solved in a simple first approximation if we neglect the relatively unimportant difference of γ_1 and γ_2 in the logarithms. By taking the representative values: $\omega_J=1.4\times10^{12}$ sec^{-1}, $I_c^0=6.8$ μA, and $\gamma\sim40$, with $\dot{I}_1=7\times10^6$ and $\dot{I}_2=0.7$ μA/sec, respectively, Eq. (14) implies that $\gamma_2\approx3\gamma_1$, or $T_1\approx3T_2$. Thus, a noise temperature roughly 3 times higher than the physical one is required in the computer simulation to compensate for the nonphysical sweep rate and give the proper reduction in the apparent I_c.

2. *Noise rounding of the high-voltage steps*

Lee[30] also derived an analytic expression for the noise rounding of the phase-locked steps in the high damping limit (β_c small). In this section, we use his results to fit the observed noise-rounded steps, using an elevated effective noise temperature to take account of shot noise, which is not included in his work.

For the nth ac-induced step, Lee's result is

$$\Delta V=\frac{2}{\gamma'}R_d I_n^0(1-e^{-\pi\gamma'\Delta\rho})T_1^{-1}[1+\beta_c'(T_2/T_1)]. \tag{15}$$

ΔV is the dc voltage measured from the step center, $\Delta\rho=\Delta I/I_n^0$, where ΔI is the current along the step measured from the step center, and I_n^0 is the step half-width without noise and R_d is the dynamic resistance at the step center without radiation. The current and voltage at the step center are I_0 and V_0, respectively, $\gamma'=\gamma(V_0/I_0R_d)$ where $\gamma=\hbar I_n^0/ekT_N^{\rm eff}$, and finally $\beta_c'=2eI_n^0R_d^2C/\hbar$. T_1 and T_2 are integrals given by

$$\begin{aligned}T_1&=\int_0^{2\pi}d\phi\,I_0[\gamma'\sin(\phi/2)]\exp(-\tfrac{1}{2}\gamma'\Delta\rho\phi)\\ T_2&=\int_0^{2\pi}d\phi\sin(\phi/2)I_1[\gamma'\sin(\phi/2)]\exp(-\tfrac{1}{2}\gamma'\Delta\rho\phi)\end{aligned} \tag{16}$$

where I_0 and I_1 are the modified Bessel functions. In the limit of $\beta_c=0$, Eq. (15) agrees with the well-known result of Ambegaokar and Halperin[31] if $\Delta\rho=I/I_c^0$, $\gamma'=\gamma=\hbar I_c^0/ekT$, $R_d=R_n$, and $\beta_c=2eI_c^0R_n^2C/\hbar$.

In their work on point contacts, Henkels and Webb[32] and Weitz *et al.*[33] used a simplified version of Eq. (15), appropriate for $\beta_c=0$, in their analyses of the noise rounding of Josephson steps at microwave and FIR frequencies, respectively. Since the Lee result[30] is valid in the limit of $\beta_c'<1$, and since $\beta_c'\sim2$ in our junctions, on the fourth step at the power level studied ($2\alpha=4.7$), it is not clear how good an approximation it will be for our data. Nonetheless this approach should give at least a rough indication of the effect of noise on the steps. In fit-

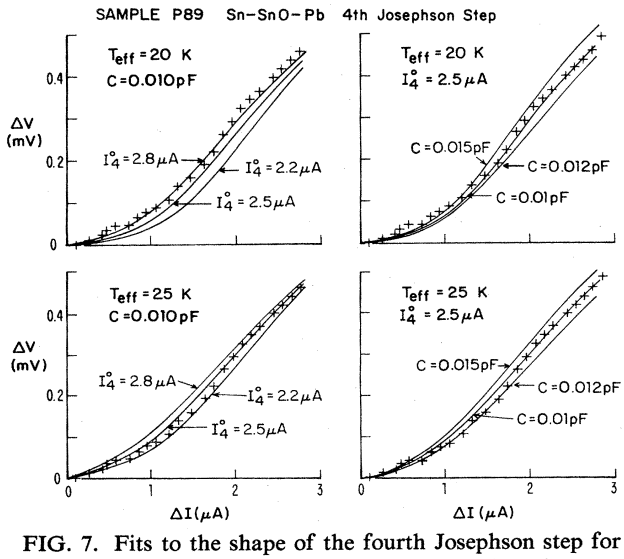

FIG. 7. Fits to the shape of the fourth Josephson step for a 176-Ω junction at 604 GHz for different values of the fitting parameters I_4^0, $T_{\rm eff}$, and C.

ting our data for the fourth step at 604 GHz (i.e., 5.0 mV), we assume a value for R_d, the dynamic resistance near the step, given by the experimental curve, and use C, $T_N^{\rm eff}$, and I_n^0 (the width of the nth step in the absence of fluctuations) as parameters. For example, as shown in Fig. 7, we obtain reasonable fits for the fourth step in our 176-Ω junction using various combinations of $C\sim 0.01-0.015$ pF, $T_N^{\rm eff}\sim 20-25$ K, and $I_4^0\sim 2.2-2.5$ μA, but wider excursions in these parameter values give significantly poorer fits. This fitted value of I_4^0 is in reasonable accordance with the value computed using the Werthamer theory and the *nominal* $I_c^0R_n$ products (~1.2 mV) determined in low R_n junctions at 1.4 K. The agreement between the fitted I_4^0 and the one calculated from the Werthamer theory is significant because the *measured* I_cR_n product is only 0.26 mV, almost a factor of 5 lower than the nominal one, and because there was no need to scale the fitted step width by the factor of ~2 used in Ref. 11. This result supports our hypothesis that the scaling factors of ~2 in the step-width fits came from approximating the normalizing denominator I_c^0 by the observed value I_c which is reduced by noise and fluctuation effects to a greater degree than is the width of the steps in the presence of strong ac-driving currents.

These results are rather interesting because the noise temperatures found, $T_N^{\rm eff}\sim 20-25$ K, are significantly higher than those found in earlier work[33] on point contacts. In those, the corresponding temperatures were $T_N^{\rm eff}\sim 10-15$ K, also on the fourth Josephson step from the 496-μm (604-GHz) laser line using the same laser setup on a point contact of similar resistance. The large difference between the two observed noise temperatures is due to different physical processes which give rise to the noise temperatures. In a *tunnel junction, shot noise* gives a mean-square noise current, $\langle i_N^2\rangle = 2eI_{\rm qp}\equiv 4kT_N^{\rm eff}/R_n$, implying $T_N^{\rm eff}=eV/2k\simeq 29$ K for $V=5.0$ mV (fourth Josephson step at 604 GHz), whereas for a *point contact,* metallic *heating* gives[20]

$$T_N^{\rm eff}\cong\tfrac{1}{2}\left[T_{\rm bath}+\frac{\sqrt{3}}{2\pi}\frac{eV}{k}\right]\cong 10\ \text{K}$$

for the same step.

C. Computer simulations

In this section we shall present the results of computer simulations of the generalized RSJ equation [Eq. (6)]. We have numerically computed representative I-V curves both with and without an applied ac current.

Although it is possible to use the full nonlinear quasiparticle tunneling curve to model $g(d\phi/d\tau)$, we have chosen instead to approximate it as follows: For voltages below $eV_g=\Delta_{\rm Sn}+\Delta_{\rm Pb}$, we use an adjustable linear leakage resistance R_L which models the usual experimental observation of excess leakage current below the gap. Above V_g, we use the full BCS quasiparticle I-V curve for $T=0$, since we will be considering experimental results far below T_c. In this manner computer execution times are made shorter, but the results of the simulation, as we will show, provide adequate quantitative comparison to the experimental results.

The noise term on the right-hand side of Eq. (6), $\hat\rho_N$, is assumed to be white noise given by the current-current autocorrelation function for a tunnel junction (for $\hbar\omega\ll eV$),[34]

$$\langle\hat I_N(t)\hat I_N(t+t')\rangle = eI_{\rm qp}(V)\coth(eV/2kT)\delta(t')\ , \tag{17}$$

where $V=V(t)=(\hbar/2e)d\phi/dt$ is the instantaneous voltage. In the computation of the *noise* current, we approximate the quasiparticle current $I_{\rm qp}(V)$ by V/R with $R=R_L$ below V_g, and simply $R=R_N$ above V_g. After conversion to the dimensionless variables used above, (17) becomes

$$\langle\hat\rho_N(\tau')\hat\rho_N(\tau+\tau')\rangle = \frac{2}{\beta_c}\frac{R}{(\hbar/e^2)}\frac{d\phi}{d\tau}\coth\left[\frac{R}{2(\hbar/e^2)}\frac{\gamma}{(\beta_c)^{1/2}}\frac{d\phi}{d\tau}\right]\hat\delta(\tau) \tag{18}$$

where $\hat\delta(\tau)$ is a dimensionless δ function. In this approximation, that $I_{\rm qp}=V/R$, Eq. (17) reduces to Johnson noise $\sim kT/R$ for $eV\ll kT$ and to shot noise $\sim eI_{\rm qp}$ for $eV\gg kT$. Note that in the shot-noise regime, i.e., $V\gtrsim 300$ μV, finite-temperature corrections cut off sharply as $e^{-eV/kT}$; in no sense is the noise a simple sum of thermal and shot-noise contributions. Accordingly, this intrinsic noise term is nearly independent of temperature over most of the I-V curve beyond the zero-voltage step. Moreover, since the instantaneous V in (17) includes the FIR drive, shot noise can dominate at high values of α even when $V_{\rm dc}=0$. As noted above, we find it necessary to introduce extrinsic noise characterized by $T_N^{\rm eff}\sim 8$ K to fit the data on the noise reduction of the observed I_c. Such extrinsic noise presumably *is* simply additive to the intrinsic noise, but is considerably smaller than the shot noise at the higher voltages where we make our most detailed comparison with experiment.

Equation (6) is solved numerically for the case of a current sweep. The method we use involves splitting the second-order Eq. (6) into two simultaneous first-order equations for ϕ and $\dot\phi$, and then applying a fourth order Runge-Kutta algorithm[35] to each. The current is incremented in fractions of the critical current, usually $\Delta\rho_{\rm dc}=0.01$. At the initial current level, e.g., $\rho_{\rm dc}=0.01$, the algorithm starts at $\tau_0=0$, with the initial conditions $\phi=\dot\phi=0$. The time increment h in units of the inverse of the plasma frequency, is typically 0.04. The algorithm waits for a period of time to permit initial transients to die out, and then the average voltage is calculated from the average of $\dot\phi$. After this, the current is incremented and the algorithm calculates ϕ and $\dot\phi$ at the new current point, using the last values of ϕ and $\dot\phi$ from the previous current point as initial conditions. The total averaging time for each current point in units of the inverse plasma frequency, $(\omega_J)^{-1}$, as typically $\sim 10^4-10^5$.

The noise term $\hat\rho_N$ is calculated using a pseudo-random-number generator to produce a noise current with zero mean and mean square given by Eq. (18). The discretization of the time variable causes the δ function to become $1/h$ when $\tau=0$, and zero otherwise, where again h is the size of the time step.

1. Computer simulations, dc case

We can now examine the results of the simulation beginning with the dc case. The method summarized by Eqs. (6) and (18) is applied here to the situation where there is no ac current, only dc current and noise, to determine the effect of noise on the critical current.

For the 176-Ω junction (P89) the simulation produces an I-V curve with the shape shown in Fig. 8(c). The dashed lines in the figure indicate the computed I_c for this junction; the variance on the computed I_c is given by the dotted-dashed lines in the figure. For comparison the experimental I-V curve is reproduced in Fig. 8(a). As noted before, the observed I_c value may be fitted to the simple thermal activation model [Eq. (7)] using $T_N^{\rm eff}=9$ K ($\gamma=36$). This can be seen from the switching probability distributions for $T_N^{\rm eff}=9$ K which are plotted in Fig. 8(b) for the experimental current sweep rate as well as for the much faster sweep rate used in the computer simulation. Going one step further, we may compare the I_c from the computer simulation Fig. 8(c) with the I_c distribution for the same fast sweep rate [Fig. 8(b)] from the thermal activation model. The agreement is reasonably good; the computer simulations yield $I_c/I_c^0=0.69\pm0.03$, whereas the thermal model gives $I_c/I_c^0=0.61\pm0.04$ at the fast sweep rate. (For comparison, $I_c/I_c^0=0.22\pm0.03$ at the slow laboratory sweep rate.) We may therefore conclude that our computer simulations of Eqs. (6) and (18) give results that are consistent with the simple thermal activation model, Eq. (7).

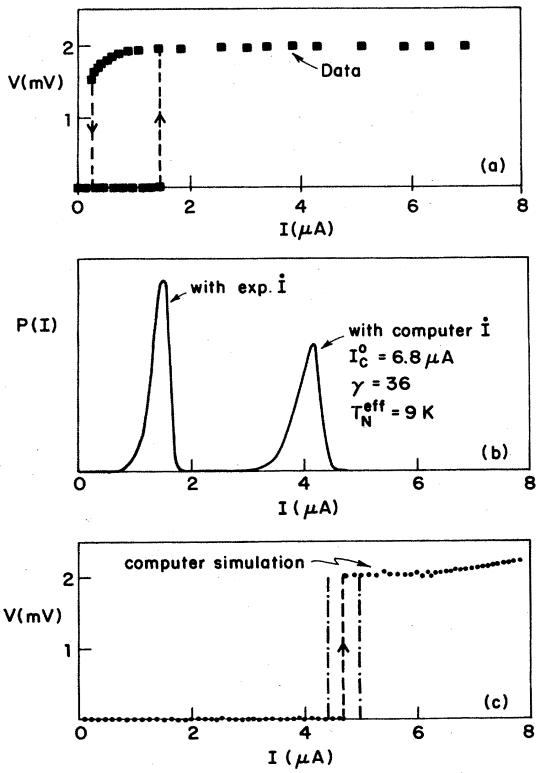

FIG. 8. (a) Experimental I-V curve at 1.4 K for the 176-Ω junction (P89) without ac bias current. (b) Switching probability distribution $P(I)$ vs I for the two relevant sweep rates, computed using transition-state theory, Eq. (10), with $T_N=9$ K. (c) Computer-simulated I-V curve for the same junction with noise current corresponding to $T_N=9$ K. Switching at the critical current is shown by the dashed line. Critical currents from the simulation (5 runs) fall within the bounds indicated by dashed-dotted lines.

For a noise temperature of 8 ± 1 K, Fig. 4 shows that this computation reproduces the observed falloff of the I_cR_n product with increasing R_n fairly well, *if* scaled to the slow laboratory sweep rate $\dot{I}$, as indicated above. The solid circles in Fig. 4 are the data from Table II, while the open circles are the results of the simulation. There is reasonably good agreement over a wide range of R_n.

2. Simulations for the FIR case

We now turn to a presentation of the simulations of the effects of the laser radiation on the junctions. Figure 9(a) shows the simulated critical current with laser power divided by the zero-power critical current *in the absence of noise,* while Fig. 9(b) display the *full* width of the first step, also in the absence of noise. I_{ab} is the step width measured by the distance in current from the point a to the point b, shown by the inset of the figure, i.e., the portion of the step on the upsweep. I_{db} labels the maximum width of the step, the region in current from d to b in the inset of the figure. We find for the finite capacitance case, $\beta_c\sim6-7$, studied in the figure, that the step widths, I_{db}, are adequately described by the Bessel-function step-width formula used before for a voltage-biased (dc and ac) RSJ-model junction:

$$I_n/I_c=|J_n(2\alpha)| \tag{19}$$

for the step half-widths. To make a comparison with the experimental data or with the simpler voltage-biased RSJ

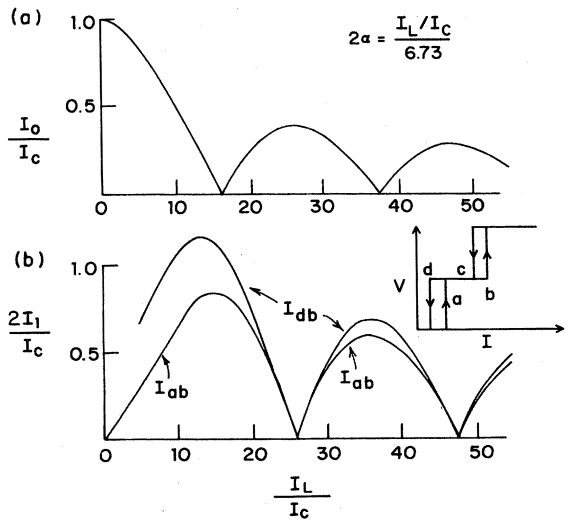

FIG. 9. Simulated step widths for a junction with ac and dc bias but *no* noise. (a) Zeroth-step half-width normalized to I_c. (b) First-step *full* width normalized to I_c. Note that if the width on the upsweep is taken, I_{ab}, the width is underestimated, whereas I_{db}, the full width of the step including the downsweep, reproduces the Bessel-function behavior.

model, we require a relationship between 2α, the normalized ac voltage in the junction (obtained from fitting to the data), and I_L/I_c, the normalized ac current used in the RSJ-model simulation. For the finite capacitance case of the RSJ model for $\Omega > 1$, a simple relationship between the two has been found by Braiman *et al.*,[36] namely

$$2\alpha = \frac{I_L/I_c^0}{\Omega(\Omega^2+\beta_c^{-1})^{1/2}} \tag{20}$$

where $\Omega = \omega_L/\omega_J$, as before. In Fig. 9 the Bessel function $|J_0(2\alpha)|$ for the zeroth step, and $|2J_1(2\alpha)|$ for the first-step full width, are indistinguishable from the lines drawn for $2\alpha = (I_L/I_c^0)/6.73$. This denominator (6.73) agrees with (20) to the precision with which ω_J is known. Figure 9(b), together with the experimental results of Fig. 3(a) of Ref. 11, indicate that it is the full width of the hysteretic step that is of importance, justifying the procedure used in the earlier work.

The effect of noise currents on the simulation is greatly modified by the presence of a strong ac drive current, as is illustrated by Fig. 10. The upper panel shows the reductions in I_c without irradiation, discussed above, which are strongly sweep-rate dependent and much greater for the noise temperature of 9 K required to fit the observation than for $T_N = 2$ K, the nominal bath temperature. By contrast, the lower panel shows the zero-voltage step at $2\alpha = 4$ (or $I_L/I_c^0 \sim 27$), where $|J_0(2\alpha)| = 0.40$ at its first secondary maximum. The solid curve shows the measured I-V curve, and the solid circles show the simulation. Within the spread of the circles, there is no distinction between the results of the simulation with $T_N = 9$ K and with $T_N = 2$ K. Although initially surprising, this result can be understood by noting that the amplitude of the noise currents is much less than the laser driving current, which also exceeds the critical current of the junction as well as the dc bias current. Whereas in the slow-sweep dc case there is time for $\sim 10^{12}$ attempts to escape the zero-voltage state, allowing infrequent extreme peaks in the weak noise currents to be effective, in the ac-driven case the situation is entirely different: only the typical rms amplitude is effective. Thus, in taking the ratio of the zeroth-step half-width I_0 with radiation to the critical current I_c, the effect of thermal noise is to reduce greatly the measured I_c, while only rounding the I-V and slightly reducing I_0, leading to an enhanced value for the ratio I_o/I_c. A similar effect occurs for the finite-voltage steps I_n. This explains the need for a scaling factor of ~ 2, essentially independent of the step number, for the Bessel and Werthamer functions used in the analysis of the FIR data of Ref. 11.

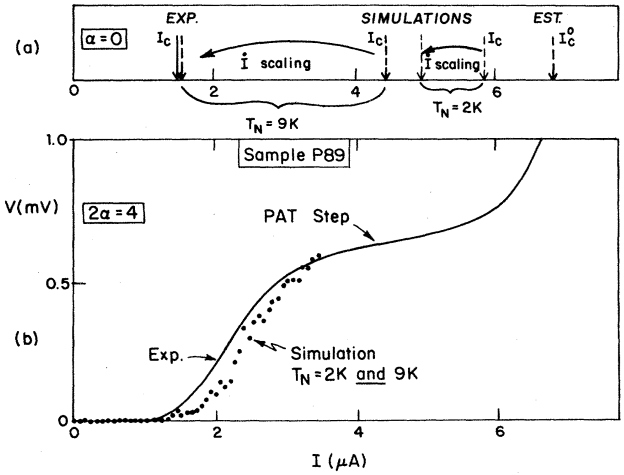

FIG. 10. Comparison between measured (full line) and simulated (solid circles) I-V curves for zeroth step with 604-GHz radiation ($2\alpha = 4.0$) on 176-Ω junction. The simulated curves for noise temperatures of 2 and 9 K coincide within the scatter of the points plotted. (The structure near 0.7 mV in the measured curve is a photon-assisted tunneling step which is not included in the simulation.) This behavior of the driven junction contrasts with that of the unirradiated junction, shown in top panel. This shows the depression of the measured I_c with T_N of 2 and 9 K, both with and without scaling to correct for the unphysically high sweep rate used in the computer simulation. In contrast to the driven case, here the noise temperature profoundly affects the simulated I_c, and 9 K is required to fit the observed I_c.

We now present our modeling of the effects of noise on the complete I-V curve of a junction at a particular laser power. We choose $2\alpha = 4.0$, the power level used in Fig. 10. We create a simulated tunnel junction I-V curve complete with photon-assisted tunneling steps and noise-rounded ac Josephson steps in the following way. First, using the simulation, we create a noise-rounded I-V curve with only Josephson steps. (As noted in connection with Fig. 10, the curve is not very sensitive to T_N.) We subtract off the smooth background as a function of voltage from this I-V curve, leaving only the local current displacements due to the ac Josephson steps. Secondly, a simulated I-V curve with only photon-assisted tunneling steps is created from the dc quasiparticle I-V curve for

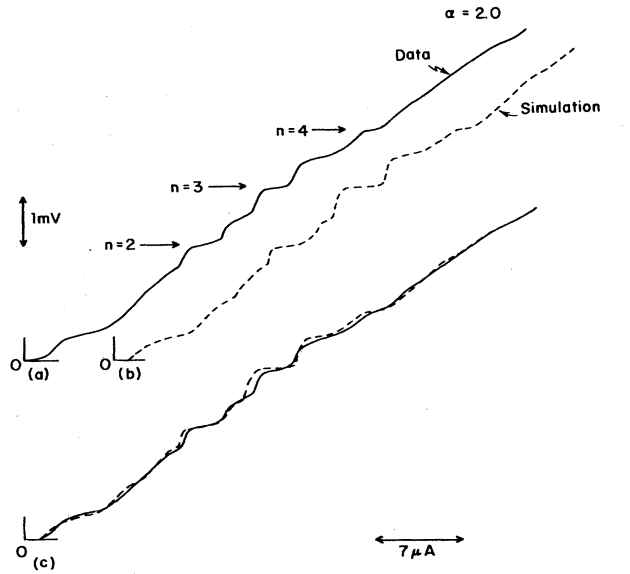

FIG. 11. (a) I-V curves of the 176-Ω junction at $2\alpha = 4.0$; Josephson steps are labeled by the integers $n = 2$, 3, and 4. (b) Simulation of the data shown in (a), which includes noise and photon-assisted tunneling steps (see text). (c) Direct comparison of simulation (b) with data (a) illustrating the quality of the fit.

this particular choice of 2α following the procedure described in Ref. 12. This I-V curve is very similar to the dashed curve for the 176-Ω junction at $\alpha=2.1$ shown in Fig. 2 of Ref. 12. Finally, the local current displacements from the ac Josephson effect are added as a function of voltage to the I-V curve with only the photon-assisted tunneling steps, creating an I-V curve with both photon-assisted steps and ac Josephson steps. The results of this procedure are shown in Figs. 11(a)—(c). In Fig. 11(a) we show the experimental I-V curve at $2\alpha=4$. The simulated I-V curve is shown in dashed lines as Fig. 11(b). In Fig. 11(c) the simulated I-V curve (dashed line) is plotted on top of the experimental I-V curve (solid line). There is a remarkable similarity between the simulation and the experimental data. The small differences may be due to the fact that the simulation does not include any effects of the frequency dependence of the step widths. That the photon-assisted tunneling and the ac Josephson effects should add in current at each voltage is precisely the expected behavior from the Werthamer result for a voltage-biased junction, further confirming that the finite capacitance makes the junction approximately voltage biased.

We can apply the above procedure in more detail to the case of the fourth step of this junction, analyzed previously[37] with the analytic approximation of Lee,[30] which ignores photon-assisted tunneling. Figure 12 displays the results of the procedure. All four curves show the fourth step, measured from the center of the step, with the data shown as a solid line, and the simulation as the solid circles. The power level is $2\alpha=4.0$ for the upper curves, while $2\alpha=5.75$ for the lower curves. Note that while the upper left ($2\alpha=4$) I-V curve fits the data very well, the lower left ($2\alpha=5.75$) simulated curve lies below the data. This suggests that the good fit at $2\alpha=4$ may be fortuitous, and affected by the contribution of the photon-assisted tunneling step which distorts the I-V curve. To explore this conjecture, on the right-half of Fig. 12 the same I-V curves are compared with simulations which now include the effects of the photon-assisted tunneling steps in addition to the noise. The resulting fit to the step data with $2\alpha=4.0$ is worse, the simulation lying below the data, while for $2\alpha=5.75$ the simulation lies much closer to the data, the net result being that both fits are of roughly comparable quality, and differ from the data in a sense that could be explained qualitatively by a higher noise temperature, or the presence of extrinsic noise. Alternatively, the frequency dependence of the Josephson current, ignored in this approximation, may need to be taken into account.

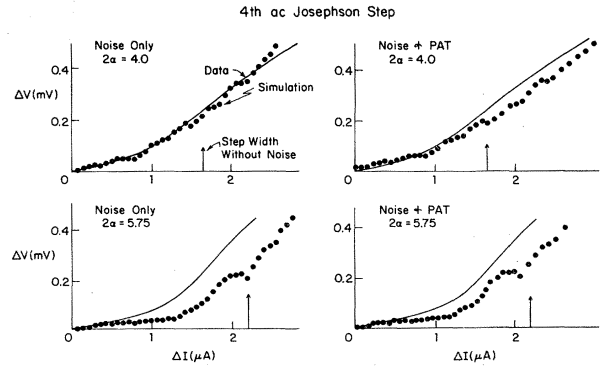

FIG. 12. Fourth Josephson-step fits at two laser-power levels, $2\alpha=4.0$, and 5.75. On the left are the simulated step shapes measured from the step center, solid circles, compared with the data, solid line. On the right is the same data, but the simulation now includes the photon-assisted tunneling effect (see text). The quality of fit for $2\alpha=4.0$ is worsened while the fit at $2\alpha=5.75$ is improved, giving roughly the same quality of fit for both, which could be improved by higher T_N.

It is remarkable that we have obtained such good fits to the data for both the falloff of the I_cR_n with increasing junction resistance and the rounding of the Josephson steps with such a simple model. We have made simplifications in treating the noise which may not be physically justified. We have taken the voltage in the noise term, $\hat{\rho}_N$, of Eqs. (6) and (18) to be the *instantaneous* voltage. This might seem dubious, because the noise power spectrum [Eq. (18)] from which the noise term, $\hat{\rho}_N$, was calculated was derived for the case of a *constant* dc bias voltage, so that it might seem more appropriate to use an average voltage to calculate the noise term. However, as a check we replaced the instantaneous voltage-dependent (shot-) noise term in the computer simulation ($\langle i_N^2\rangle \sim 2eV/R_n$) by a Johnson noise term ($\langle i_N^2\rangle = 4kT_N^{\rm eff}/R_n$) at an elevated temperature, $T_N^{\rm eff}=eV/2k\sim 30$ K, appropriate to the fourth step at 5.0 mV (604 GHz), and found that the simulated step shape with this noise temperature was nearly identical to that simulated before with the voltage-dependent noise term. Also, the white-noise approximation used is questionable because of the very broad bandwidth response of these junctions. In any case we have found rather remarkable agreement between our data and the RSJ simulations used, which gives some credibility to the method.

V. DISCUSSION AND CONCLUSIONS

Before concluding this paper we would like to briefly point out some recent analytic approaches to the problem of noise in junctions which go beyond the now classic results utilized here.

In a recent paper Ben-Jacob *et al.*[38] have examined the effects of shot noise on the nonzero voltage state of a hysteretic junction and found a distribution of fluctuations that is nonsymmetric in that positive fluctuations are more probable than negative ones. Their results are confined to the hysteretic region of the junction I-V curve, and are applicable for $\beta_c > 1.6$, but not too large, and could be tested by observing the transition rate to the zero-voltage state from the nonzero-voltage state.

Büttiker, Harris, and Landauer[39] have extended to a broader range of β_c the treatment of the noise-activated escape of a particle out of a metastable well given originally by Kramers,[40] and applied to superconducting tunnel junctions by Lee[30] for the extreme underdamped case ($\beta_c \gg 1$). Using the theory of Büttiker *et al.* to calculate the most likely observed switching current for our junctions, we find only negligibly small corrections ($<0.1\%$ change) to the results of the simple transition-state model used above.

The theoretical developments cited above are applicable to shunted junctions and only in certain limits of parameters. These analyses have not been extended to the case of a junction with the full *nonlinearity* of the quasiparticle I-V curve, nor a junction which is driven by a FIR or microwave source. Recently, several groups[41–43] have used path integral formalisms to treat the problem of the transition out of the zero-voltage state when thermally activated processes are frozen out. These treatments can take the full nonlinearity of the quasiparticle I-V curve into account, but physically intuitive results, or results for junctions driven by high-frequency sources, are not yet available.

We conclude this work by observing that we have found good agreement between the falloff of the measured I_cR_n product of small-area superconducting tunnel junctions and the predictions of the simple analytic result derived using an estimate of the lifetime of the junction in its zero-voltage state in the presence of thermal activation corresponding to a noise temperature $T_N^{\rm eff} \approx 8$ K, taking account of the actual laboratory sweep rate $\dot{I}$. For computational reasons, a parallel computer-model simulation employed a current sweep rate about 10^7 times faster, which gives a much smaller depression of I_c for a given T_N. However, the depression predicted by this simulation is in good agreement with that predicted by the analytic model when the computer sweep rate is also used in the latter. Thus the models give results which are consistent with each other, and with experiment if an elevated effective noise temperature of ~ 8 K is used. This noise is probably due to external sources, although considerable pains have been taken to minimize extrinsic noise coupling into the junction circuit. Unfortunately, the open geometry and antenna structure required to allow coupling of FIR radiation to the junction in our experiments precludes use of geometries in which the junction is totally enclosed in metal shielding; with such geometries, other workers have been able to observe intrinsic thermal noise effects even at $T \lesssim 1$ K.

In the presence of strong FIR currents coupled into the junctions, quite different conditions prevail. Thermal noise currents have much less effect, so that simulations for $T_N^{\rm eff}$ of 2 and 9 K are not significantly different. As a result, the width I_0 of the zero-voltage step at the first subsidiary maximum of the Bessel-function dependence can be *greater* than the fluctuation-reduced I_c, rather than only 40% of I_c as would be expected in the absence of the reduction of I_c by fluctuations. For the high-voltage steps, shot noise dominates, and the computer simulation and the data agree quite well. Reasonable fits to the observed rounding of the step widths at $V \approx 5$ mV can also be obtained using the analytic result of Lee, applicable to $\beta_c < 1$, but using an elevated noise temperature of ~ 25 K to model the effect of shot noise (for $V \approx 5$ mV), which is not included in that model.

ACKNOWLEDGMENTS

We would like to acknowledge helpful discussion about this work with Professor John Clarke and Dr. Gerd Schön. One of us (J.B.H.) acknowledges the generous support of the Carlsberg Foundation and of the North Atlantic Treaty Organization (NATO) Science Fellowship Program while this work was being done. This work was supported in part by U.S. Joint Services Electronics Program Contract No. N00014-75-C-0648 and U.S. Office of Naval Research Contracts Nos. N00014-83-K-0383 and N00014-79-6-066.

*Present address: Physics Department, University of California, Berkeley, CA 94720.

†Present address: H. C. Ørsted Institute, University of Copenhagen, DK-2100 Copenhagen Ø, Denmark.

‡Present address: Fundación Instituto de Ingeniera, Apartado Postal 1827, Caracas 1010A, Venezuela.

§Present address: Research Division, Polaroid Corporation, Cambridge, MA 02139.

[1]P. L. Richards, in *Semiconductors and Semimetals,* edited by R. K. Willardson and A. C. Beers (Academic, New York, 1977), Vol. 12, Chap. 6; IEEE Trans. Electron Devices, **ED—27**, 1909 (1980); see also T. G. Phillips and G. J. Dolan, Physica **109—110B&C**, 2010 (1982).

[2]J. T. Anderson and A. M. Goldman, Physica **55**, 256 (1971).

[3]M. Simmonds and W. H. Parker, Phys. Rev. Lett. **24**, 876 (1970).

[4]C. M. Falco, W. H. Parker, S. E. Trullinger, and P. K. Hansma, Phys. Rev. B **10**, 1865 (1974).

[5]G. Hawkins and J. Clarke, J. Appl. Phys. **47**, 1616 (1976).

[6]C. T. Rogers and R. Buhrman, IEEE Trans. Mag. **MAG—19**, 453 (1983).

[7]R. H. Koch, D. J. Van Harlingen, and J. Clarke, Phys. Rev. Lett. **47**, 1216 (1981).

[8]T. Fulton and L. N. Dunkleberger, Phys. Rev. B **9**, 4760 (1974).

[9]R. F. Voss and R. A. Webb, Phys. Rev. Lett. **47**, 265 (1981).

[10]L. D. Jackel, J. P. Gordon, E. L. Hu, R. E. Howard, L. A. Fetter, D. M. Tennant, R. W. Epworth, and J. Kurkijarvi, Phys. Rev. Lett. **47**, 697 (1981).

[11]W. C. Danchi, F. Habbal, and M. Tinkham, Appl. Phys. Lett. **41**, 883 (1982).

[12]F. Habbal, W. C. Danchi, and M. Tinkham, Appl. Phys. Lett. **42**, 296 (1983).

[13]G. J. Dolan, Appl. Phys. Lett. **31**, 337 (1977).

[14]L. N. Dunkleberger, J. Vac. Sci. Technol. **15**, 88 (1978).

[15]R. E. Howard, E. L. Hu, L. D. Jackel, L. A. Fetter, and R. H. Bosworth, Appl. Phys. Lett. **35**, 879 (1979).

[16]K. Mizuno, Y. Daiku, and S. Ono, IEEE Trans. Microwave Theory and Tech. **MTT—25**, 470 (1977).

[17]T. G. Blaney, National Physical Laboratory (Teddington, U.K.) Report No. 89/0382, March 1978 (unpublished).

[18]W. C. Jakes, Jr., in *Antenna Engineering Handbook,* edited by H. Jasik (McGraw-Hill, New York, 1961), Chap. 10.

[19]G. C. Southworth, *Principles and Applications of Waveguide Transmission* (Van Nostrand, New York, 1950), Chap. 5.

[20]D. A. Weitz, Harvard University (Division of Applied Sciences) Technical Report No. 14, Tinkham Series, May 1978 (unpublished).

[21]D. A. Weitz, W. J. Skocpol, and M. Tinkham, Opt. Lett. **3**, 13 (1978).

[22]T. C. Wang and R. I. Gayley, Phys. Rev. B **18**, 293 (1978).
[23]A. Barone and G. Paterno, *Physics and Applications of the Josephson Effect* (Wiley, New York, 1982), Chap. 1.
[24]M. Tinkham, *Introduction to Superconductivity* (McGraw-Hill, New York, 1975), p. 35.
[25]E. P. Balsalmo, G. Paterno, A. Barone, P. Rissman, and M. Russo, Phys. Rev. B **10**, 1881 (1974); also A. Barone and G. Paterno, *Physics and Applications of the Josephson Effect,* Ref. 23, p. 200.
[26]D. A. Weitz, W. J. Skocpol, and M. Tinkham, Appl. Phys. Lett. **31**, 227 (1978).
[27]D. A. Weitz, W. J. Skocpol, and M. Tinkham, J. Appl. Phys. **49**, 4873 (1978).
[28]P. K. Tien and J. P. Gordon, Phys. Rev. **129**, 647 (1963).
[29]B. D. Josephson, Phys. Lett. **1**, 251 (1962).
[30]P. A. Lee, J. Appl. Phys. **42**, 325 (1971).
[31]V. Ambegaokar and B. I. Halperin, Phys. Rev. Lett. **10**, 486 (1969).
[32]W. H. Henkels and W. W. Webb, Phys. Rev. Lett. **26**, 1164 (1971).
[33]D. A. Weitz, W. J. Skocpol, and M. Tinkham, Phys. Rev. B **18**, 3282 (1978).
[34]A. J. Dahm, A. Denenstein, D. N. Langenberg, W. H. Parker, D. Rogovin, and D. J. Scalapino, Phys. Rev. Lett. **22**, 1416 (1969).
[35]*Handbook of Applicable Mathematics, Vol. III: Numerical Methods,* edited by R. F. Churchhouse (Wiley, New York, 1981), p. 321.
[36]Y. Braiman, E. Ben-Jacob, and Y. Imry, in *Proceedings of the IC SQUID Conference, Berlin, 1980,* edited by H. D. Halbohm, (Walter de Gruyter and Co., New York, 1980), p. 783.
[37]W. C. Danchi, F. Habbal, and M. Tinkham, IEEE Trans. Magn. **MAG—19**, 498 (1983).
[38]E. Ben-Jacob, D. J. Bergman, Y. Imry, B. J. Matkowsky, and Z. Schuss, Appl. Phys. Lett. **42**, 1045 (1983).
[39]M. Büttiker, E. P. Harris, and R. Landauer, Phys. Rev. B **28**, 1268 (1983).
[40]H. A. Kramers, Physica **7**, 284 (1940).
[41]A. O. Caldeira and A. J. Leggett, Phys. Rev. Lett. **46**, 211 (1981).
[42]S. Chakravarty, Phys. Rev. Lett. **49**, 681 (1982).
[43]V. Ambegaokar, U. Eckern, and G. Schön, Phys. Rev. Lett. **48**, 1745 (1982).